0026-895X/07/7203-592–603$20.00
MOLECULAR PHARMACOLOGY
Vol. 72, No. 3
38398/3247039
Mol Pharmacol 72:592–603, 2007
Printed in U.S.A.

Human Pregnane X Receptor Antagonists and Agonists Define Molecular Requirements for Different Binding Sites[S]

Sean Ekins, Cheng Chang,[1] Sridhar Mani, Matthew D. Krasowski, Erica J. Reschly, Manisha Iyer, Vladyslav Kholodovych, Ni Ai, William J. Welsh, Michael Sinz, Peter W. Swaan, Rachana Patel,[2] and Kenneth Bachmann

ACT LLC, Jenkintown, Pennsylvania (S.E.); Department of Pharmaceutical Sciences, University of Maryland, Baltimore, Maryland (S.E., C.C., P.W.S.); Albert Einstein Cancer Center and Department of Medicine, Albert Einstein College of Medicine, Bronx, New York (S.M.); Department of Pathology, University of Pittsburgh Medical Center, Pittsburgh, Pennsylvania (M.D.K., E.J.R., M.I.); Department of Pharmacology, University of Medicine and Dentistry of New Jersey, Robert Wood Johnson Medical School, Piscataway, New Jersey (V.K., N.A., W.J.W.); Bristol-Myers Squibb Company, Research Parkway, Wallingford, Connecticut (M.S.); and Department of Pharmacology, The University of Toledo, Toledo,Ohio (R.P., K.B.)

Received May 22, 2007; accepted June 18, 2007

ABSTRACT

The pregnane X receptor (PXR) is an important transcriptional regulator of the expression of xenobiotic metabolism and transporter genes. The receptor is promiscuous, binding many structural classes of molecules that act as agonists at the ligand-binding domain, triggering up-regulation of genes, increasing the metabolism and excretion of therapeutic agents, and causing drug-drug interactions. It has been suggested that human PXR antagonists represent a means to counteract such interactions. Several azoles have been hypothesized to bind the activation function-2 (AF-2) surface on the exterior of PXR when agonists are concurrently bound in the ligand-binding domain. In the present study, we have derived novel computational models for PXR agonists using different series of imidazoles, steroids, and a set of diverse molecules with experimental PXR agonist binding data. We have additionally defined a novel pharmacophore for the steroidal agonist site. All agonist pharmacophores showed that hydrophobic features are predominant. In contrast, a qualitative comparison with the corresponding PXR antagonist pharmacophore models using azoles and biphenyls showed that they are smaller and hydrophobic with increased emphasis on hydrogen bonding features. Azole antagonists were docked into a proposed hydrophobic binding pocket on the outer surface at the AF-2 site and fitted comfortably, making interactions with key amino acids involved in charge clamping. Combining computational and experimental data for different classes of molecules provided strong evidence for agonists and antagonists binding distinct regions on PXR. These observations bear significant implications for future discovery of molecules that are more selective and potent antagonists.

M.D.K. is supported by grant K08-GM074238 from the National Institutes of Health and a Competitive Medical Research Fund grant from the University of Pittsburgh Medical Center. M.I. received support from a University of Pittsburgh Pathology Postdoctoral Research Training Program. S.M. was supported by the Damon Runyan Cancer Research Foundation (C1:15-02) N.A, V. K., and W.J.W. were supported by the United States Environmental Protection Agency-funded Environmental Bioinformatics and Computational Toxicology Center (ebCTC), under STAR Grant number GAD R 832721-010.

S.E., C.C., and S.M. contributed equally to this work.

Current affiliation: Pharmacokinetics, Dynamics, and Metabolism, Pfizer, Groton, CT.

Current affiliation: Sun Pharmaceutical Industries Inc., Bryan, Ohio.

Article, publication date, and citation information can be found at http://molpharm.aspetjournals.org.
doi:10.1124/mol.107.038398.

[S] The online version of this article (available at http://molpharm.aspetjournals.org) contains supplemental material.

The human pregnane X receptor [PXR (NR1I2; also known as SXR or PAR)] is a transcriptional regulator of the enzymes CYP3A4 (Bertilsson et al., 1998; Blumberg et al., 1998; Kliewer et al., 1998), CYP2B6 (Goodwin et al., 2001), and CYP2C9 as well as many other enzymes and transporters, such as P-glycoprotein (ABCB1) (Synold et al., 2001), and proteins involved in the transport, metabolism, and biosynthesis of bile acids (Staudinger et al., 2001a,b). These discoveries have shown how drugs may regulate not only their own metabolism but potentially also their own efflux, as demonstrated for paclitaxel (Schuetz and Strom, 2001). Overall, there is an incredibly broad structural diversity in the mol-

ABBREVIATIONS: PXR, pregnane X receptor; LBD, ligand-binding domain; AF-2, activation function-2; LXR, liver X receptor; T-0901317, *N*-(2,2,2-trifluoroethyl)-*N*-{4-[2,2,2-trifluoro-1-hydroxy-1-(trifluoromethyl)ethyl]phenyl}benzenesulfonamide; ET-743, trabectedin; SMRT, silencing mediator for retinoid and thyroid receptors; QSAR, quantitative structure-activity relationship; PLS, partial least-squares; L-742694, 2-((3,5-bis(trifluoromethyl)benzyl)oxy)-3-phenyl-4-((3-oxo-1,2,4-triazol-5-yl)methyl)morpholine; CoMFA, comparative molecular field analysis; DMSO, dimethyl sulfoxide; MTT, 3-(4,5-dimethylthiazol-2-yl)-2,5-diphenyltetrazolium bromide; PRESS, predictive error sum of squares; CB, chlorobiphenyl; SR12813, [2-(3,5-di-*tert*-butyl-4-hydroxy-phenyl)-1-(diethoxy-phosphoryl)-vinyl]-phosphonic acid diethyl ester.

ecules that bind to human PXR in vitro, and this has not yet been summarized extensively in reviews. A small sample of the molecules published and suggested to bind PXR include: bile salts (Schuetz and Strom, 2001; Krasowski et al., 2005a), cholesterol and its metabolites (Sonoda et al., 2005), statins (El-Sankary et al., 2001), endocrine disruptors (Takeshita et al., 2001, 2006), synthetic peptide bond mimetics (Mu et al., 2005), anticancer compounds (Mani et al., 2005), herbal components and plant extracts (Moore et al., 2000; Ding and Staudinger, 2005; Mu et al., 2006), carotenoids (Rühl et al., 2004, 2005), vitamins (Zhou et al., 2004), HIV protease inhibitors (Dussault et al., 2001), calcium channel modulators (Drocourt et al., 2001), steroids (Moore and Kliewer, 2000), plasticizers (Masuyama et al., 2000, 2002; Takeshita et al., 2001), pesticides (Coumol et al., 2002; Lemaire et al., 2004), peroxisome proliferator-activated receptor-γ antagonists (Leesnitzer et al., 2002), as well as other diverse xenobiotics and endobiotics (Lehmann et al., 1998; Waxman, 1999; Ekins and Erickson, 2002; Luo et al., 2002; Schuster et al., 2006; Ung et al., 2007), including agonists for additional nuclear receptors (Xue et al., 2007a).

X-ray crystallography of the ligand-binding domain (LBD) of PXR (Watkins et al., 2001, 2002, 2003a,b) suggests that it is a large, flexible mostly hydrophobic site with some key polar residues. A recent cocrystal structure indicates 17β-estradiol bridges between the polar residues Ser247 and Arg410 and represents overlapping interactions with the previous crystal structures for more diverse molecules (Xue et al., 2007b). Binding of the coactivator SRC-1 to activation function-2 (AF-2) on the surface of PXR is key for stabilizing the receptor (Watkins et al., 2003a). A recent X-ray crystallographic structure of PXR with the liver X receptor (LXR) agonist *N*-(2,2,2-trifluoroethyl)-*N*-{4-[2,2,2-trifluoro-1-hydroxy-1-(trifluoromethyl)ethyl] phenyl} benzenesulfonamide (T-0901317) was employed to examine potential PXR antagonists that bind in the LBD (Xue et al., 2007a). The authors concluded that because of the flexibility and promiscuity of the LBD, identifying such antagonists might be difficult. Known antagonists for PXR include ET-743 (Synold et al., 2001), polychlorinated biphenyls (Tabb et al., 2004), and some azoles (Takeshita et al., 2002; Huang et al., 2007; Wang et al., 2007). For example, Takeshita et al. (2002) showed that ketoconazole disrupted the corepressor silencing mediator for retinoid and thyroid receptors (SMRT) receptors as well as SRC-1 from binding with PXR. Ketoconazole (Huang et al., 2007), fluconazole (Wang et al., 2007), and enilconazole (Wang et al., 2007) have been shown to inhibit the activation of PXR in the presence of paclitaxel, whereas the azoles are themselves weak agonists on their own. Ketoconazole inhibits the PXR-SRC-1 interaction and is therefore likely to bind the AF-2 site; however, it failed to antagonize a double mutant T248E/K277Q PXR, which may be due to the synergistic effects of these two residues (i.e., creating a site for a lower level coactivator binding than that seen in the wild type). These mutations are in the AF-2 binding pocket and not in the ligand binding pocket, which implies that the original residues lysine and threonine (which lie in the AF-2 side) must be important for ketoconazole binding and inhibitory interaction (Wang et al., 2007). This led the authors to speculate that ketoconazole mimics the histidine residue of SRC-1 in interacting at the AF-2 site. The isothiocyanate sulforaphane, a dietary compound found in broccoli, was recently shown to function as a PXR antagonist by displacing ligands from the LBD and inhibiting PXR-coactivator recruitment (Zhou et al., 2007). It is noteworthy that this represents the first naturally occurring human PXR antagonist.

The clinical implications of modulating the transcription of drug-metabolizing enzymes and transporters via PXR are therefore important for minimizing drug-drug interactions. In view of the wide array of molecules that bind PXR, our ability to predict potential interactions and adverse drug reactions that may accelerate clearance of drugs and, consequently, diminish efficacy (Zhou et al., 2007) is critical for drug discovery and development, as well as for toxicology assessment. Several predictive computational models for PXR have been developed to define key features of ligands that bind (Ekins and Erickson, 2002; Bachmann et al., 2004; Schuster et al., 2006). Most pharmacophore models feature four to five hydrophobic features and at least one to two hydrogen-bonding moieties. In addition, a statistical quantitative structure-activity relationship (QSAR) model, using VolSurf descriptors and partial least-squares (PLS), that identified hydrogen bond acceptor regions and amide responsive regions was described for 33 PXR ligands, although no test set data were provided (Jacobs, 2004). A second statistical model using a recursive partitioning method has been used with 99 PXR activators and nonactivators to predict the probability of aprepitant, L-742694, 4-hydroxytamoxifen, and artemisinin binding to PXR (Ekins et al., 2006). Additional models based on machine learning methods using a set of PXR activators and nonactivators (Ung et al., 2007) displayed overall prediction accuracies between 72 and ~80%, whereas an external test set of known activators had a similar level of accuracy. So far, we are not aware of the application of ligand-based or protein-based methods for modeling PXR antagonists.

The novel aims of the current study were to use a combination of in vitro data and computational methods [pharmacophores, comparative molecular field analysis (CoMFA)] for PXR agonists and antagonists to define the important features and locations for binding and to answer the question of whether the PXR antagonists assessed bind in the LBD or at the AF-2 site. Finally, we have used a structure-based docking method to position azole antagonists and further support our ligand-based approaches to rationalize the in vitro data and previously published mutagenesis study (Wang et al., 2007). This research represents the first combined computational modeling of PXR antagonists and different series of PXR agonists.

Materials and Methods

Reagents and Plasmids

The DPX-2 cell line was a gift from Puracyp Inc. (Carlsbad, CA). The corresponding dosing and culturing media were also purchased from Puracyp Inc. The construction of the HepG2 (human liver) cells stably expressing human SLC10A1, a transporter that can take up conjugated bile salts, has been reported previously in detail (Krasowski et al., 2005a). Human PXR was expressed as a full-length protein, and CYP3A4-PXRE-Luc, which contains promoter elements from CYP3A4 recognized by the PXR DNA-binding domain, was used as the reporter construct. The plasmids for human PXR, human SLCO1A2, CYP3A4-PXRE-Luc, and empty vectors pSG5 were generously provided by S.A. Kliewer, J. T. Moore, and L. B. Moore

(GlaxoSmithKline, Research Triangle Park, NC). Clotrimazole, mifepristone, androstenol, pregnenolone 16α-carbonitrile, rifampicin, and sterile filtered dimethyl sulfoxide (DMSO) were purchased from Sigma-Aldrich (St. Louis, MO). 5α-Petromyzonol and allocholic acid were obtained from Toronto Research Chemicals (North York, ON, Canada). All other steroids and bile salts were purchased from Steraloids (Newport, RI). Tissue culture petri dishes were acquired from VWR International (West Chester, PA). Opaque, tissue culture-treated, sterile white 96-well plates were purchased from PerkinElmer Life and Analytical Sciences (Waltham, MA). Clear-bottomed, tissue culture-treated, sterile white 96-well plates were purchased from Fisher Scientific (Pittsburgh, PA). The Steady-Glo Luciferase Assay System to measure induction, the CellTiter-Glo Luminescent Cell Viability Assay System, and all other laboratory equipment required for cell culture were purchased from Fisher Scientific.

Reporter Gene Assay with DPX-2 Cells

The protocols describing the cell culture techniques and standard operating procedures for the reporter gene assay, obtained from Puracyp Inc., were accurately followed. The tissue culture protocols were performed in the sterile laminar flow hood. All incubations were carried out at 37°C and 5% CO_2.

The DPX-2 cells were obtained frozen in liquid nitrogen. After successful cell plating and generation of a viable cell line, media was aspirated and replaced every 2 days until the cells reached 70 to 80% confluence. The medium was aspirated, and cells were rinsed with 5 ml of PBS. PBS was replaced with 2 ml of trypsin/EDTA and incubated for 5 min. Two milliliters of medium was added, and the entire mixture was transferred to a 15-ml centrifuge tube. Cells were pelleted at 500 rpm for 3 min and re-suspended in 5 ml of culture medium. The cell density was determined using 0.4% trypan blue in sterile filtered PBS and a Brightline Hemocytometer. The cells were diluted to achieve the desired concentration. Cell suspension (100 μl) corresponding to 30,000 cells was added to each well of a 96-well plate, using a 12 channel pipettor and special wide-bore pipette tips. The plates were incubated overnight. Drug stock solutions (10 mM for each compound) were prepared in DMSO and diluted directly into the dosing medium. The final DMSO concentration of 0.1% was maintained in all dilutions. DPX-2 cells plated in 96-well dishes were treated with selected inducers by replacing the medium in each well with 150 μl of media containing an appropriate concentration of inducer or DMSO control; each condition was repeated in quadruplicate. Thereafter, each plate examining the test compounds was also treated with 10 μM rifampicin, mifepristone, and androstenol as known comparators of varying effectiveness (potent, moderate, or weak) for PXR activation. Test articles included clotrimazole and eight novel azole compounds: CDD3501, CDD3508, CDD3530, CDD3532, CDD3536, CDD3538, CDD3540, and CDD3543. Apart from rifampicin, which was tested at 0.5, 1, 5, 10, 15, 20, 25, and 30 μM, all other compounds were diluted to 0.1, 0.5, 1, 5, 10, 15, and 20 μM from the stock solution. After a 24-h treatment, cell medium containing test compound or DMSO was aspirated from the wells and frozen for future analysis. Room temperature Dulbeccos' phosphate-buffered saline (100 μl) was added to each well because it contains calcium and magnesium ions necessary for the luminescence assay. Promega SteadyGlo Luciferase reagent and Cell Titer-Glo Viability reagent were prepared as per manufacturer's protocol by combining the substrate buffer solution with the lyophilized substrate solution. The induction/viability reagent (100 μl) was added to the designated plates and mixed thoroughly by pipetting up and down five times. Induction and viability assays were conducted in separate plates because the strong luminescence associated with the viability assay interfered with the luminescence obtained with induction. The plates were placed away from light to allow for dark adaptation. They were sealed with self-adhesive clear plastic sheets and luminescence was quantified on the TopCount NXT. The TopCount was normalized and adjusted to detect luminescence in each well for 30 s.

Reporter Gene Assay with HepG2 Cells

PXR activation in the HepG2 human liver cell line was determined by a luciferase-based reporter assay as described previously (Krasowski et al., 2005b). The basic method for the luciferase reporter assays in 96-well format was as follows. HepG2-SLC10A1 cells were grown in modified Eagle's medium-α containing 10% fetal bovine serum and 1% penicillin/streptomycin (Invitrogen, Carlsbad, CA) at 37°C in 5% CO_2. On day 1, cells were seeded onto 96-well opaque white plates at 30,000 cells/well. On day 2, the medium was exchanged, and cells were transfected using calcium phosphate precipitation. For experiments involving human PXR, 25 ng/well of CYP3A4-PXRE-Luc reporter, 2.7 ng/well human PXR (in pSG5 plasmid), and 20 ng/well pSV-β-galactosidase (Promega, Madison, WI) were cotransfected. For experiments involving sulfated steroids or bile salts, human SLCO1A2 was cotransfected at 10 ng/well to facilitate uptake of sulfated compounds. On day 3, the cells were washed with Hanks' buffered salt solution (Invitrogen) and then exposed to media containing the test molecules or vehicle to be tested. The medium used charcoal-dextran-treated fetal bovine serum (Hyclone, Logan, UT) to reduce background activation. Cells were washed once with Hanks' buffered salt solution and then lysed with 150 μl of lysis buffer (Reporter Lysis Buffer; Promega, Madison, WI). Separate aliquots were taken for measurement of β-galactosidase activity (Promega) and luciferase activity (Steady-Glo; Promega). Each drug concentration was performed at least in quadruplicate and repeated in separate experiments for a total of at least three times. Data are expressed as mean ± S.D. Complete concentration-response data were collected for all compounds with at least eight concentrations per compound tested. Some of the data for the bile salts have been previously reported (Krasowski et al., 2005a).

To test for cytotoxicity, two assays that have been well validated in HepG2 cells were used: 3-(4,5-dimethylthiazol-2-yl)-2,5-diphenyltetrazolium bromide (MTT) reduction and Alamar blue reduction. Both assays sensitively measure the ability of viable cells to metabolize the parent compound to a metabolite that can be detected by spectrophotometry or fluorometry (Hamid et al., 2004). HepG2 cells were seeded at a density of 20,000 cells/well (100 μl per well) into clear 96-well microplates (for the MTT assay) or black, opaque 96-well plates (for the Alamar blue assay) and grown for 24 h. The next day, 100-μl solutions of drug concentrations or vehicle controls in cell growth medium at twice the intended final concentration were added to the cells (final volume, 200 μl). The cells were again incubated for 24 h. For the MTT assays, MTT (in vitro toxicology assay kit, MTT-based; Sigma, St. Louis, MO) was dissolved at 5 mg/ml in warm cell growth medium. This solution (20 μl) was added to the cells (total volume, 220 μl), and the plates were incubated for another 4 h. After incubation, the supernatant was removed and 50 μl of solubilization buffer provided in the Sigma kit with 0.5% DMSO was added. DMSO was added to ensure total solubility of the formazan crystals. Plates were shaken for 2 min, and the absorbance was recorded at 590 nm. The percentage viability was expressed as absorbance in the presence of test compound as a percentage of that in the vehicle control (with subtraction of background absorbance).

For the Alamar blue assays, Alamar blue stock solution (Biosource International, Camarillo, CA) was diluted 1:1 with cell growth medium, and 50 μl of this was added to each well, yielding a final concentration of 10% Alamar blue (total volume, 250 μl). The plates were exposed to an excitation wavelength of 530 nm, and the emission at 590 nm was recorded to determine whether any of the test drug concentrations fluoresce at the emission wavelength. Plates were returned to the incubator for 5 h, and the fluorescence was measured again. The percentage viability was expressed as fluorescence counts in the presence of test compound as a percentage of that in the vehicle control (with subtraction of background fluorescence). Drug concentrations that cause >30% loss of cell viability in the

MTT assay or >15% loss of cell viability in the Alamar blue assay were not used in the determination of concentration-response curves for activation of PXRs.

Data Generation for PXR Antagonists

The assays used to generate the effect of azole and imidazole antagonists for PXR have been described previously in detail and the reader is referred to these (Mani et al., 2005; Huang et al., 2007; Wang et al., 2007).

Statistical Analyses

Dose response curves were plotted for each imidazole compound tested, including the positive controls using Kaleidagraph Software (Synergy Software, Reading, PA). The equation for the logistic dose-response curve was represented by the rearranged form of the Hill equation:

$$E = 1 + \left[\frac{C^n(E_{max} - 1)}{C^n + C_{50}^n}\right] \quad (1)$$

Dose response curves were additionally plotted using the E_{max} model equation:

$$E = \left(\frac{[C]^* E_{max}}{[C] + EC_{50}}\right) \quad (2)$$

For the E_{max} model, curves were forced to plateau for the three controls, rifampicin, mifepristone, and androstenol, by artificially setting an E_{max} at the average of the highest consistent -fold induction values.

-Fold induction was calculated as the ratio of the luminescence obtained with treatment of test compound compared with treatment with 0.1% DMSO (control). The control was added to each 96-well plate to account for any interplate variability. The raw data were appropriately labeled. Of the four replicates performed for each assay point, any one replicate was discarded if it deviated significantly (greater than 1-fold) from the other three results. The average of the DMSO replicates was calculated, and this represented the negative control. The average of each dilution of each control and test article was calculated, along with the average of the media-only replicates (no DMSO). The media-only average represented the background control and helped to determine whether the DMSO had deteriorated. The average was used for comparison with DMSO: if it lay within 10% of the DMSO reading, it was discarded. -Fold induction for each dilution of controls and test articles was calculated by dividing the average of the test results by the average of the negative control. For clotrimazole, final induction data were represented by the average of 3 distinct assays. Figures for each data point were normalized to viability. For viability, results were expressed as -fold induction in viable cells. The number of viable cells was determined as a ratio to DMSO-treated cells.

For the steroidal compounds, concentration response curves were fitted using Kaleidagraph. The relative efficacies (ε) for each compound are the maximal response of the test ligand divided by the maximal response obtained with 10 μM rifampicin. Compounds with $\varepsilon < 0.05$ were considered "inactive." All comparisons with maximal activators were done within the same microplate.

In Silico Modeling

Catalyst. The computational molecular modeling studies were carried out using Catalyst version 4.9 (Accelrys, San Diego, CA) running on an SGI Octane workstation (SGI, Palo Alto, CA). Pharmacophore models attempt to describe the arrangement of key features that are important for biological activity. In brief, the Catalyst models were employed to generate hypotheses. After sketching the molecules in Catalyst, the 3-D molecular structures were produced using up to 255 conformers with the BEST conformer generation method, allowing a maximum energy difference of 20 kcal/mol. A Hypogen PXR agonist pharmacophore was generated with Catalyst using the steroidal agonist data derived from HepG2 cells in this study and recently published data for 31 diverse molecules with EC_{50} values (Sinz et al., 2006) (Supplemental Table 1). Ten hypotheses were generated using these conformers for each of the molecules and the EC_{50} values, after selection of the following features: hydrophobic, hydrogen bond acceptor, hydrogen bond donor, and ring aromatic features. After assessing all 10 generated hypotheses, the hypothesis with lowest energy cost was selected for further analysis because this possessed features representative of all the hypotheses and had the lowest total cost. The quality of the structure activity correlation between the estimated and observed activity values was estimated by means of an r value.

When the set of molecules was too small for a Hypogen model, HipHop was used to align the molecules, which is independent of biological activity. Catalyst was used to generate a common features (HipHop) (Clement and Mehl, 2000) pharmacophore. Up to 255 conformers were generated for each molecule with the BEST conformer generation method, allowing a maximum energy of 20 kcal/mol. A HipHop pharmacophore for the imidazole PXR agonists (Table 1, Fig. 1) was generated from alignment of all 8 CDD compounds and clotrimazole. All molecules were aligned to the clotrimazole structure. For the equipotent (~10 μM) PXR antagonists enilconazole, ketoconazole, and fluconazole (Huang et al., 2007), a HipHop pharmacophore was generated. In this case, the template molecule was

TABLE 1

Imidazole agonists with experimental PXR data and predictions

Side-by-side comparison of E_{max} and EC_{50} values were obtained utilizing the two dose response curve modeling equations and the experimental E_{max} values. E_{max} refers to the maximum increase in -fold induction obtained when DPX-2 cells were treated with PXR agonists over cells treated with the negative control, 0.1% DMSO. The experimental E_{max} is the highest observed -fold induction for each compound. The -fold induction results were corrected for cell viability and represent the mean of three or four determinations. For further experimental details, see *Materials and Methods*.

Compound	Prediction from Bachmann et al. (2004)	Via Simple E_{max} Model		Via Hill's Model		Experimental E_{max}	
		E_{max}	EC_{50}	E_{max}	EC_{50}	Concentration	E_{max}
	μM		μM		μM	μM	
Rifampicin		33.9	4.1	35	4.7	20	31
Mifepristone		16.2	3.1	16.5	4	10	15.3
Androstenol		9.9	1.9	9	1.8	10	8.8
CDD3501		22.4	2.3	19	1.8	10	20.3
CDD3508		36	4.1	34	3.9	10	29.7
CDD3530		26.6	3.6	22.5	3.1	10	24
CDD3532		20.6	1.5	20.9	2	20	20.2
Clotrimazole		16	0.8	15	0.8	20	16.2
CDD3536		24	2.4	24.2	2.5	20	22.2
CDD3538	9.6	30.2	1.3	27.8	1.1	10	30.9
CDD3540	25	31.5	2.3	26.9	1.7	10	32.7
CDD3543	3.4	25.7	1.4	25.1	1.4	10	25.7

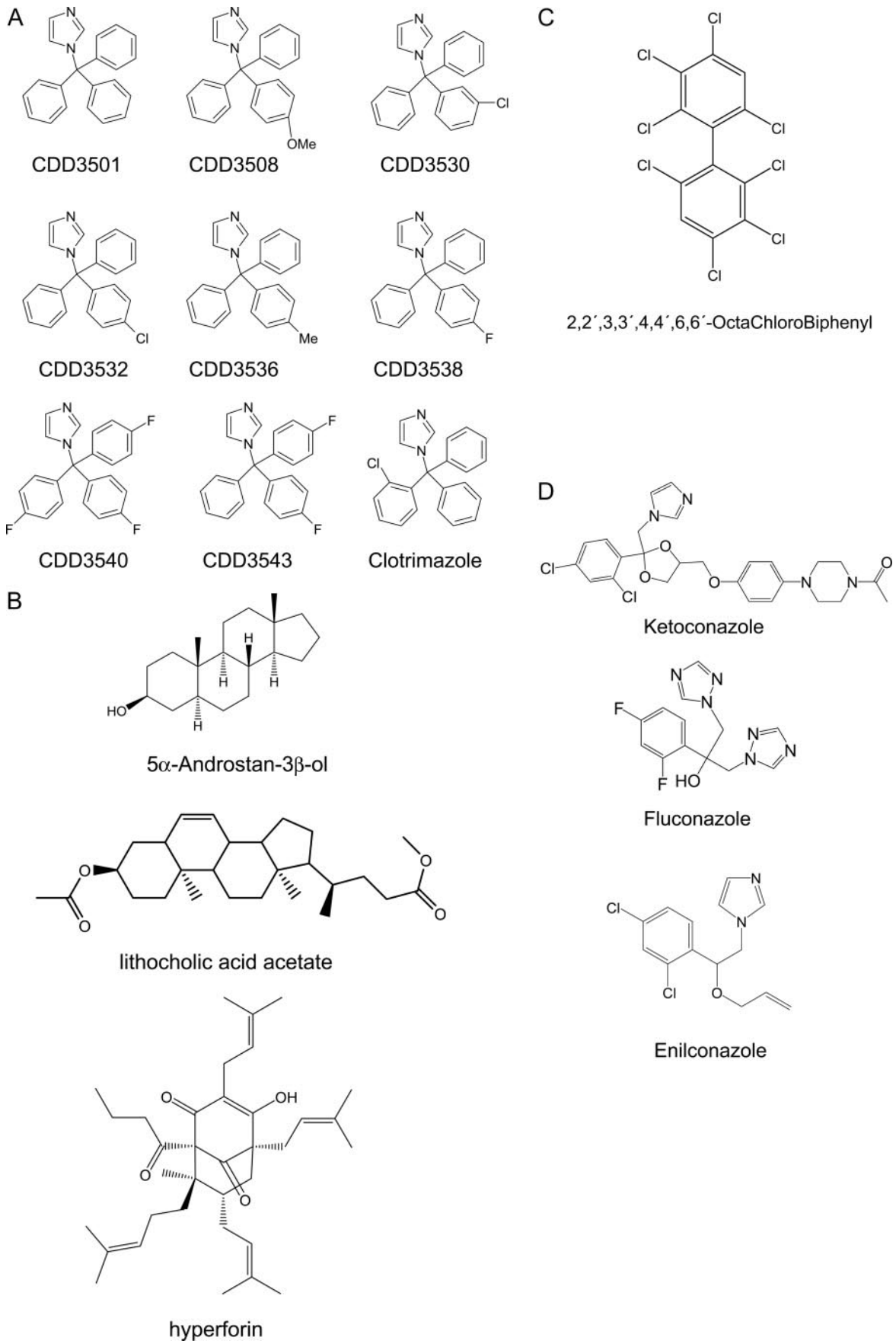

Fig. 1. Structures of selected PXR agonists and antagonists. A, imidazoles (Bachmann et al., 2004). B, steroidal molecules and hyperforin (Sinz et al., 2006). C, 2,2′,3,3′,4,4′,6,6′-octachlorobiphenyl (Tabb et al., 2004). D, azoles (Wang et al., 2007).

ketoconazole, to which the other two molecules were aligned. Molecules were then aligned using hydrophobic, hydrogen bond acceptor, hydrogen bond donor, and ring aromatic features.

CoMFA. CoMFA (Tripos, St. Louis, MO) is a widely applied QSAR method that attempts to explain the gradual changes in observed biologic properties by evaluating the electrostatic (Coulombic interactions) and steric (van der Waals interactions) fields at regularly spaced grid points surrounding a set of mutually aligned structures (Cramer et al., 1988).

Of all the aspects required for CoMFA modeling, correctly aligned structures is most essential to ensure successful and meaningful model results; hence, this method is generally used with homologous structural series. For the imidazole agonist data set, the clotrimazole structure was first sketched in Sybyl (Tripos) using standard bond distances and lengths. After initial optimization, systematic search was performed, allowing all flexible bonds to rotate with 10° increments. The conformation with lowest energy from systematic search was further optimized using energy minimization. The final optimized structure was used as a scaffold for the generation and optimization of all other imidazole derivatives. All structures were aligned according to the central carbon atom and the four anchoring points of the phenyl groups.

Nineteen differently substituted polychlorinated biphenyls that were previously suggested as human PXR antagonists (Tabb et al., 2004) were also analyzed separately using CoMFA (Supplemental Table 2). The molecules were similarly sketched and optimized in Sybyl. The backbone alignment was straightforward because all structures possess identical rigid backbone structures. Care was taken to ensure that the chlorinated sites on each molecule maximally overlapped those on the other molecules.

In all cases, electrostatic and steric interaction fields were calculated using an sp3 hybridized carbon probe atom (+1 charge at 1.52 Å van der Waals radius) on a 2.0-Å spaced lattice, which extends beyond the dimensions of each structure by 4.0 Å in all directions. A cutoff of 30 kcal/mol ensures that no extreme energy terms will distort the final model. The indicator fields and hydrogen bond fields generated by the advanced CoMFA module were also included in the analysis. To eliminate excessive noise, all electrostatic interaction energies below 1.0 kcal/mol and steric interaction energies below 10.0 kcal/mol were set to zero. PLS was used to correlate the field descriptors with biologic activities. CoMFA descriptors were used as independent variables, whereas the dependent variable (biologic descriptor) used in these studies was $-\text{LogEC}_{50}$ (imidazole agonists) and $-\text{Log}K_i$ (polychlorinated biphenyl data). The predictive value of the models was evaluated first using leave-one-out cross-validation. The cross-validated standard coefficient, q^2, was calculated as follows:

$$q^2 = 1 - \frac{\sum_Y (Y_{\text{predicted}} - Y_{\text{observed}})^2}{\sum_Y (Y_{\text{observed}} - Y_{\text{mean}})^2} \quad (3)$$

where $Y_{\text{predicted}}$, Y_{observed}, and Y_{mean} are the predicted, observed, and mean values of the target property ($-\text{LogEC}_{50}$ or $-\text{Log}K_i$), respectively. $\Sigma(Y_{\text{predicted}} - Y_{\text{observed}})^2$ is the predictive error sum of squares (PRESS). The standard error of the cross-validated predictions is represented as *press*, whereas the root-mean-square value of the conventional (noncross-validated) analysis is known as *s*. The model with the optimum number of PLS components, corresponding to the lowest PRESS value, was selected to derive the final PLS regression model. In addition to the q^2, the conventional correlation coefficient r^2 and its standard error were also calculated. A plot of predicted versus experimental activity was used to identify potential outliers. The process was repeated until no further improvements in q^2 or no outliers could be identified. Results from alternative descriptor fields were compared, and the model with the highest q^2 was selected for later analysis. A contour plot of standard coefficients enclosing the highest 20% value was created for each model [except the electrostatic positive favorable interaction (blue contour) for the imidazole agonist model, where the top 10% values were plotted for clarity]. The contours of the steric map are shown in yellow and green, whereas the contours of the electrostatic map are shown in red and blue. Greater activities (lower EC_{50} values for PXR agonists and lower K_i values for PXR antagonists) are correlated with less bulk near yellow areas, whereas more bulk is tolerated near green areas. More negative charge is preferred near red regions, whereas more positive charge is needed near blue regions.

Docking Antagonists to the Crystal Structure Using GOLD. Protein preparation for GOLD docking (Jones et al., 1997) was done in Sybyl 7.2. From the Protein Data Bank entry 1NRL and the larger fragment of chain A, Ser192-Gly433 was chosen for a protein site preparation. Water molecules, salt ions, ligands, and coreceptor fragments were deleted. Only hydrogen position energy optimization was performed after addition of hydrogen atoms and assigning of the AMBER 02 force-field charges to the protein. The resulting protein was saved in Tripos mol2 format and used later as a docking site in GOLD.

The 1NRL chain A was used for rigid docking in which the protein was fixed and only flexibility was allowed for ligands. Each ligand was set to dock 20 times. Automatic cavity detection around Glu427, approximately x 1.345, y 20.932, z 18.464, was performed on chain A with a 15-Å radius to make sure all atoms of the SRC-1 binding groove were covered. This was termed site 1. GOLD also explores adjunct regions for docking. A second docking site (site 2) was defined around the atom on the protruding tip of SRC-1, x 3.582, y 16.389, z 21.454 with a radius of 5 Å only.

Results

Imidazole PXR Agonist Pharmacophore. The first published PXR pharmacophore (Ekins and Erickson, 2002) generated with EC_{50} data for 12 agonists had previously been used to predict human PXR interactions for three imidazoles that were shown to increase apoA1 and HDL-C in rodents (Bachmann et al., 2004) (Table 1). These predictions suggested that the molecules were likely to be agonists. The experimental data from this current study confirm that all three molecules are indeed low micromolar agonists of human PXR in DPX-2 cells (Table 1). In addition, a luciferase-based reporter assay was performed using HepG2 cells, as described previously (Zhu et al., 2004), and an 11-point dose-response curve from 2.5 to 50 μM, and this also demonstrated that four of the novel imidazoles and clotrimazole were low micromolar agonists of human PXR (Table 2). These same molecules also behaved as antagonists as they were also competitive inhibitors of rifampicin binding, indicating that they were probably binding in the LBD. The imidazoles were found not to be cytotoxic in this reporter assay (data not shown).

As the computational predictions for the novel imidazoles binding to human PXR as agonists diverged from the experimental data in terms of the ranking, this necessitated the generation of a separate pharmacophore for the 9 imidazoles used in this study, which were all found to have low micromolar affinity but with a range of E_{max} values (with some molecules with comparable efficacy to rifampicin). Because there was not the required 3-log unit variation in biological activity necessary for Hypogen pharmacophore generation, we opted to align the compounds using common features. The common features HipHop pharmacophore consisted of three ring aromatic (hydrophobes) and a single hydrogen bond acceptor (Fig. 2A). The mapping of these molecules is similar

TABLE 2

Imidazoles with PXR transactivation agonist and antagonist data from HepG2 cells

The luciferase based reporter assay was performed using HepG2 cells as described previously (Zhu et al., 2004) using an 11-point dose-response curve from 2.5 to 50 μM. Maximum activation observed is percentage of rifampicin response at 10 μM. For further experimental details, see *Materials and Methods*.

Compound	Luciferase-DMSO (Agonist Mode)		Luciferase-Rifampicin (Antagonist Mode)	
	EC_{50}	Maximum Activation Observed	EC_{50}	Maximum Activation Observed
	μM	%	μM	%
CDD3508	4.4	73	23.9	108
CDD3530	1.5	70	14.3	110
CDD3532	1.3	81	14.4	110
CDD3538	1.4	92	18.4	108
CDD3540	1.9	56	15.8	110
Clotrimazole	1.1	96	16.7	107

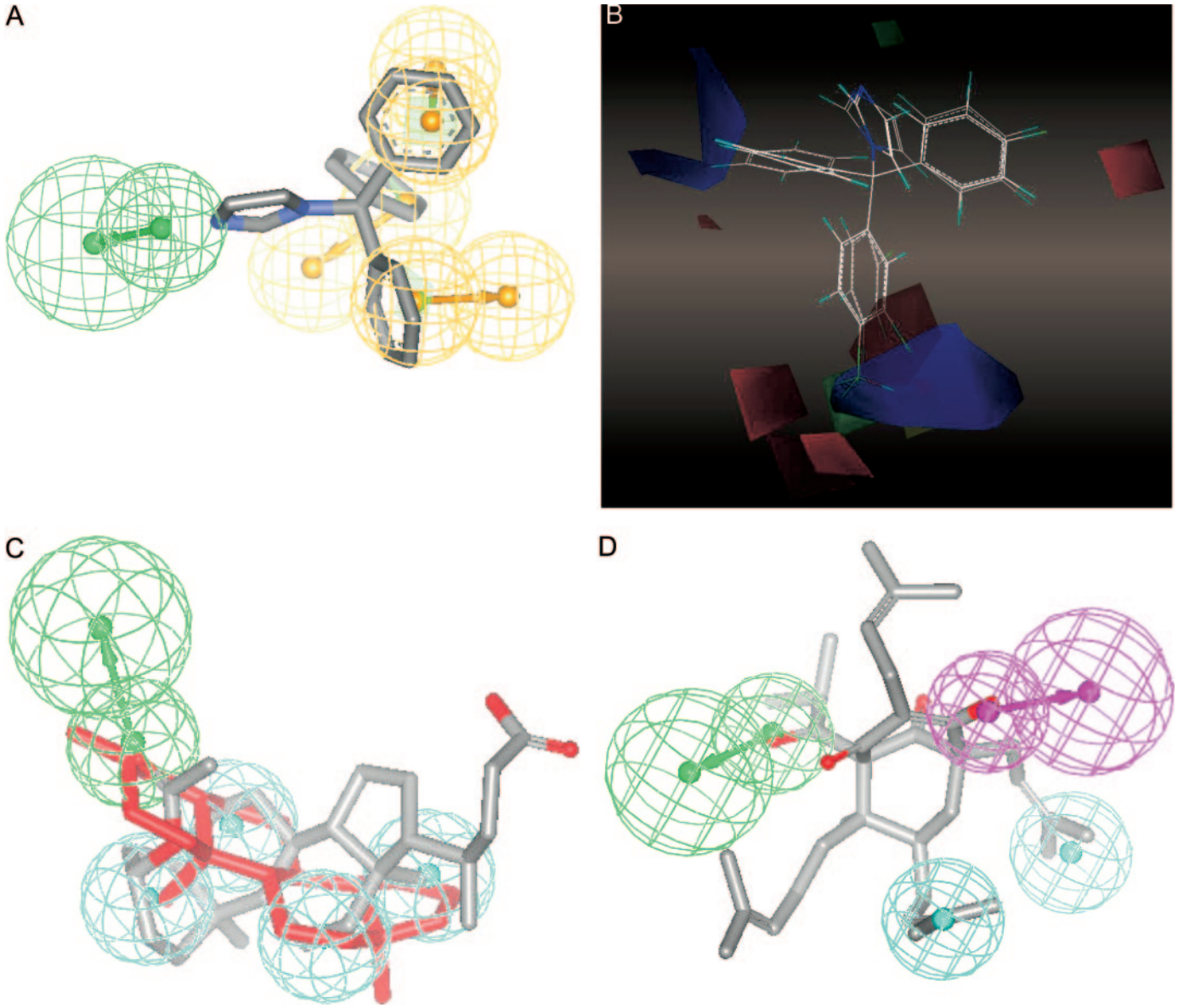

Fig. 2. PXR agonist models. A, azole PXR agonist HipHop pharmacophore, showing CDD3501 aligned to ring aromatic features (brown) and a hydrogen bond acceptor (green). B, azole PXR agonist CoMFA model with coefficient contour map aligned with all training set compounds. C, steroidal PXR pharmacophore: The pharmacophore possessed one hydrogen bond acceptor (green) and four hydrophobes (cyan). Aligned are the two most active compounds, 5α-androstan-3β-ol (red) and lithocholic acid acetate (gray), showing the mapping to these features. D, diverse PXR agonist Hypogen pharmacophore showing hyperforin aligned to hydrophobes (cyan), hydrogen bond acceptor (green), and hydrogen bond donor (purple) features.

to the previously observed alignment to three of the four hydrophobes in the original PXR pharmacophore from which our initial predictions were derived (Bachmann et al., 2004).

Imidazole PXR Agonist CoMFA Analysis. A highly consistent and predictive PXR agonist model was developed after removing CCD3508 as an outlier. The leave-one-out cross-validated r^2 (q^2) is 0.527 with a PRESS value of 0.24 using five principle components. The CoMFA model revealed that contributions were greater from steric (59%) interactions than from electrostatic (41%) interactions. As shown in Fig. 2B, multiple red contours covering the lower benzene group illustrate the favorable substitution of halogen atoms on this ring, thus introducing more negative charge. This explains the higher affinity of clotrimazole, CDD3538 and CDD3532. The blue contour over the *meta* position of the benzene group indicates substitution with a more negative charge at this position is not favorable for PXR activation, as exemplified by the weaker agonist CDD3530 (EC_{50} value: 3.05 μM). The blue contour over the para position of the left ring also indicates that a negative charge at this position is not favorable, whereas the red contour over the *para* position of the right ring indicates the favorable substitution of chlorine at this position for PXR activation. These two different correlations may reflect the affinities of CDD3540 (1.72 μM) and CDD3543 (1.44 μM).

Steroidal PXR Agonist Pharmacophore. The PXR activation data for 30 steroidal molecules include data for nine bile salts that were part of a previous study comparing PXR ligand activation across animal species (Krasowski et al., 2005a). The steroidal ligands possessed a wide EC_{50} range (0.8–104 μM with 9 inactives, Table 3) that was used to derive a Catalyst Hypogen model with an observed versus predicted correlation $r = 0.75$. The difference between the total cost of the model and the null cost can be used as an additional indicator of model significance. In this case, the total cost of 182.175 compared with null total cost of 248.114 represents an acceptable cost difference compared with previously published Catalyst models (Ekins and Erickson, 2002). The pharmacophore possessed one hydrogen bond acceptor (green) and four hydrophobes (Fig. 2C, cyan). Aligned to this pharmacophore are the two most active compounds 5α-androstan-3β-ol (red) and lithocholic acid acetate (gray) showing the mapping to these features.

Diverse PXR Agonist Pharmacophore. The 31 diverse published molecules with EC_{50} data (range, 0.04–39 μM) resulted in a Catalyst Hypogen model with an observed versus predicted correlation $r = 0.855$. However, the total cost of 133.5 compared with the null cost of 135.7 does not represent a significant difference in this case. This model consists of two hydrophobes, one hydrogen bond acceptor, and one hydrogen bond donor (Fig. 2D).

Biphenyl PXR Antagonist CoMFA. The iterative analysis during the CoMFA model generation process identified 2,2′,3,3′,4,4′,6-hepta-chlorobiphenyl (CB), 2,2′,4,4′,5,5′-hexa-CB, and 2,2′,3,4,4′,5,5′,6-octa-CB as outliers and excluded them from the final result. The final antagonist model has a similar predictive power as the imidazole agonist CoMFA model, with a q^2 of 0.573 and PRESS of 0.377 using five principle components. Both steric and electrostatic interactions contributed to the final model (53 and 47%, respectively). The CoMFA coefficient contour map aligned with the most potent compound, 2,2′,3,3′,4,4′,6,6′-octa-CB, is shown in Fig. 3A. This is dominated by red contours surrounding both phenyl rings and reflects the favorable chlorine substitutions on both rings. The presence of a blue contour over the 5 position of the left phenyl ring is the result of absence of a chlorine atom at this position among the most active antagonists.

Azole PXR Antagonist Pharmacophore. Enilconazole and fluconazole were aligned to ketoconazole using HipHop because they are all suggested to possess similar antagonist activity with PXR (Wang et al., 2007). The resulting pharmacophore contained two hydrogen bond acceptor features, a hydrophobe, and a ring aromatic (hydrophobic) feature (Fig. 3B).

Docking of Azole Antagonists. The results from GOLD docking the three azoles in PXR are shown in Fig. 4, A and B. We identified two separate locations on either side of Lys277, and in both cases, binding of azoles would interfere with SRC-1 binding in the AF-2 site. The GOLD docking scores for binding at site 1 with enilconazole (43.07), fluconazole (44.46), and ketoconazole (58.41), are higher than at site two with enilconazole (39.13), fluconazole (36.27), and ketoconazole (50.68). The higher score represents a higher predicted affinity for the protein. It was noted that the alignment of ketoconazole to the other two azoles may not be optimal at site 1 (not shown), because they do not seem to overlap as one would expect based on their similar antagonist activity (Huang et al., 2007). In contrast, at site 2, the azoles overlap

TABLE 3

Concentration response data for steroidal ligands activating human PXR in HepG2 cells

PXR activation in the HepG2 human liver cell line was determined by a luciferase-based reporter assay as described previously (Krasowski et al., 2005b). Each drug concentration was performed at least in quadruplicate and repeated in separate experiments for a total of at least three times. Data are expressed as mean ± S.D. For further experimental details, see *Materials and Methods*.

Compound Name	EC_{50}	Efficacy
	μM	
17β-dihydroandrosterone	4.15 ± 0.2	0.68
Androstanol	6.27 ± 0.3	0.5
Dihydrotestosterone	11.4 ± 0.5	0.39
Etiocholanolone	5.7 ± 0.6	0.54
5β-Cholan-3α,7α,12α,24-tetrol	>100	0
Taurochenodeoxycholic acid[a]	104 ± 8	0.5
Deoxycholic acid[a]	50.2 ± 4.5	0.19
Lithocholic acid[a]	10 ± 0.1	0.15
7-Ketolithocholic acid[a]	21.5 ± 1.4	0.58
12-Ketolithocholic acid[a]	31.3 ± 5.8	0.86
ω-Muricholic acid[a]	>100	0
Taurocholic acid[a]	>100	0
Cholesterol	>100	0
Estradiol	16 ± 0.1	0.34
Estrone	37.9 ± 3.3	0.47
Estriol	>100	0
5β-Pregnane-3,20-dione	2.6 ± 0.2	0.97
17-Hydroxyprogesterone	17.7 ± 2.3	0.7
Petromyzonol[a]	>100	0
Allocholic acid[a]	>100	0
PCN	>100	0
Cortolone	44.7 ± 7.4	0.72
Estetrol	2.14 ± 0.2	0.29
Epitestosterone sulfate	3.39 ± 0.7	0.67
5β-Pregnan-3α,20β,diol	3.81 ± 0.3	0.49
5α-Androstan-3β-ol	0.8 ± 0.01	0.43
16,(5α)-Androsten-3β-ol	4.77 ± 1.0	1.01
5β-Androstan-3α-ol	1.41 ± 0.1	1.12
Tauro-β-muricholic acid[a]	>100	0
Lithocholic acid acetate[a]	1.2 ± 0.2	0.54

[a] Published previously (Krasowski et al., 2005a).

in a manner similar to that of the Catalyst antagonist pharmacophore (Fig. 3B). The site 2 is predominantly hydrophobic. It consists of 15 amino acids. Lys252, Ile255, Lys259, Pro423, Leu424, Glu427, and Leu428 form one side of the groove and are responsible for accommodation of the dichlorophenyl group of ketoconazole. Phe264, Ile269, Glu270, Gln272, Ile273, Ser274, and Leu276 are on the other side of the binding pocket and contribute to the interaction with the azole ring and other heterocyclic groups of the ketoconazole. Lys277 most likely serves as a "charge clamp" for interaction between the coactivator SRC1 (His687) and PXR, and it probably plays a significant role on the initial phase of accommodating azoles in the binding groove of PXR.

Discussion

Qualitative Computational Comparisons of PXR Agonist and Antagonist Models. There have been attempts to model PXR agonists using computational methods such as pharmacophores (Ekins and Erickson, 2002; Ekins et al., 2002; Bachmann et al., 2004; Schuster et al., 2006), QSAR (Jacobs, 2004; Ekins et al., 2006; Ung et al., 2007), and homology modeling with molecular dynamics (Wang et al., 2006). These generally made use of data from different experimental groups and did not computationally model PXR antagonism, focus on limited structural types for agonists, or assess potential binding sites using such methods. From the various PXR agonist pharmacophores and computational models developed in this study using data from our own laboratories and that published elsewhere (Tabb et al., 2004; Sinz et al., 2006), a consensus emerges that agonists—whether imidazole, steroidal, or more diverse structures—are required to fit to multiple hydrophobic features and one hydrogen bond acceptor. For example, the imidazole pharmacophore contains three hydrophobic ring aromatic features (Fig. 2A), and the CoMFA model for imidazole agonists shows a larger contribution of steric versus electrostatic fields (Fig. 2B), which is in agreement with the role of hydrophobic interactions for agonists. We have also identified a novel PXR agonist steroidal pharmacophore that contains four hydrophobes (Fig. 2C), whereas the diverse molecule pharmacophore contains 2 hydrophobic features (Fig. 2D). All of these pharmacophores also possess one hydrogen bond acceptor. These results are generally in close accord with the previous PXR agonist pharmacophores (Ekins and Erickson, 2002; Schuster et al., 2006) and crystal structures. In particular, the steroidal pharmacophore contains most of the features recently reported with the crystal structure using 17β-estradiol, indicating one of the two hydrogen bond acceptors, as well as the hydrophobic interactions of the A and B rings

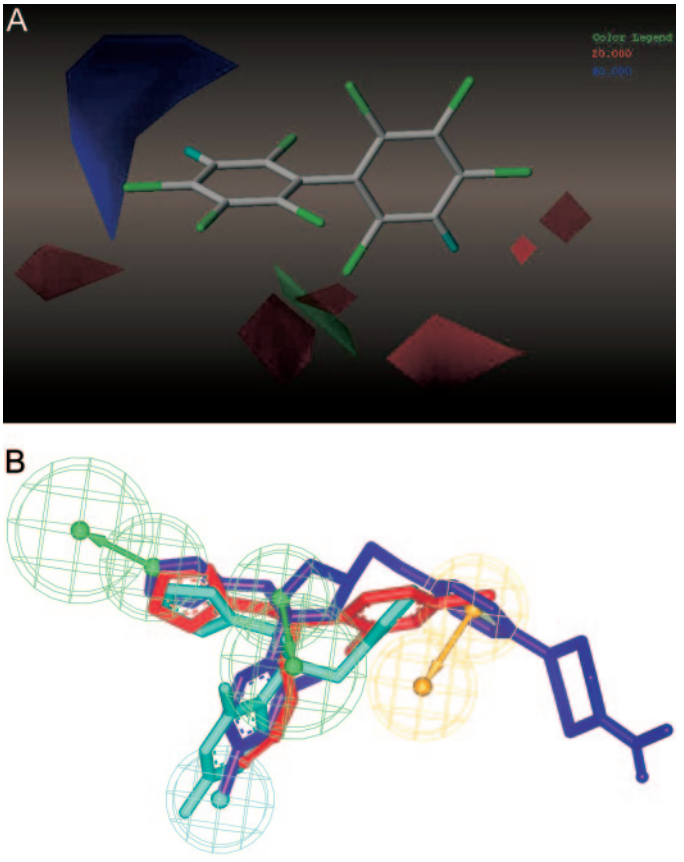

Fig. 3. PXR antagonist models. A, biphenol PXR antagonist CoMFA model showing coefficient contour map aligned with the most active biphenyl 2,2′,3,3′,4,4′,6,6′-octachlorobiphenyl. B, imidazole PXR antagonist HipHop pharmacophore. A, enilconazole (red), ketoconazole (purple), and fluconazole (cyan) mapped to hydrogen bond acceptors (green), hydrophobic (cyan), and ring aromatic features (orange).

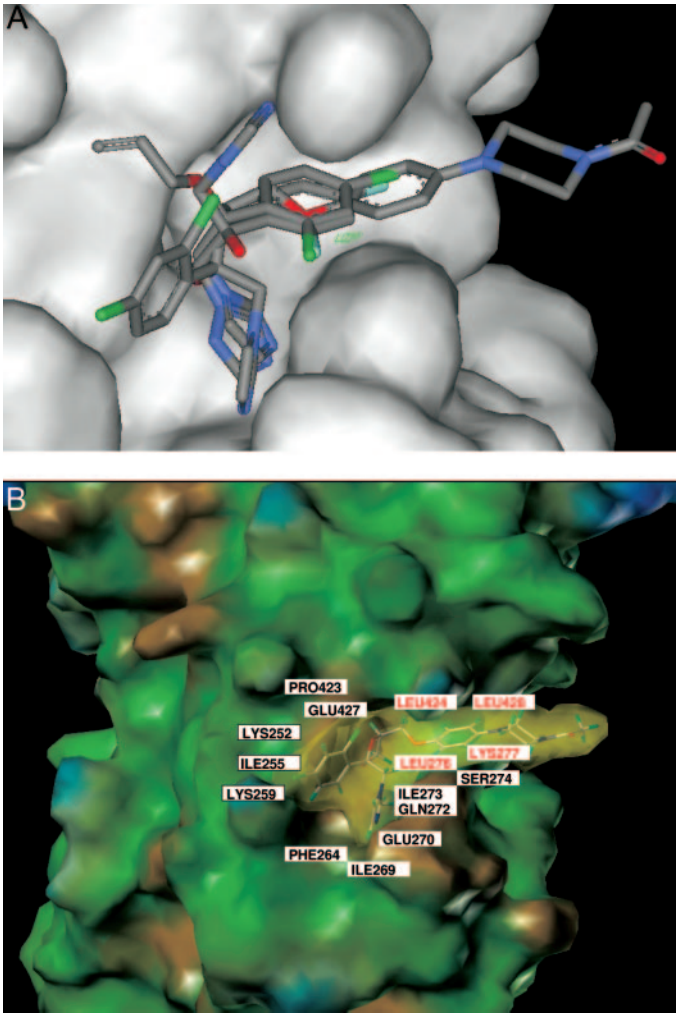

Fig. 4. Docking of azoles in PXR 1NRL using GOLD. A, all azole antagonists align well in the binding site 2 and the piperazine ring of ketoconazole is exposed to solvent. B, ketoconazole with van der Waals surface showing the fit into the binding pocket.

(Xue et al., 2007b). The training set for this model also contains 17β-estradiol with an EC_{50} of 16 μM, close to that previously reported in the X-ray crystallography study (20 μM). However, it should be noted that the most active compound, 5α-androstan-3β-ol, with an EC_{50} value of 0.8 μM, has a single hydrogen bond acceptor feature; therefore, both hydrogen bonds in the crystal structure may not be necessary for other steroidal ligands to bind PXR. It should also be noted that the more diverse molecule pharmacophore contains an additional hydrogen bond donor feature but does not possess optimal cost difference values and requires further evaluation. In addition, although previous pharmacophore models have suggested multiple hydrogen bond acceptors (Schuster et al., 2006) a role for a hydrogen bond donor has not been noted (Ekins and Erickson, 2002; Schuster et al., 2006). This would suggest that the two most active molecules in this diverse molecule pharmacophore, SR12813 and hyperforin, which both have a single hydroxyl functional group, are aligning their ring features. The hydroxyl on SR12813 was shown to form a π-stacking interaction with Trp299 in the 1NRL crystal structure (Watkins et al., 2003a), providing direct evidence of an important hydrogen bonding interaction that was missed previously when the same two molecules were superimposed (Schuster et al., 2006). An additional observation from this study is the dependence of the resulting agonist pharmacophore on the types of molecules used in the training set, indicating that there may be numerous potential models that partially overlap.

In contrast, the PXR antagonist CoMFA model based on biphenyls seems to have a lower steric and higher electrostatic contribution than those of the imidazole agonist CoMFA model. The antagonist model is also noticeably smaller (Fig. 3A). It has previously been suggested that the substitution patterns that maximize antagonism also maximize hydrophobic features on rings in a square-square pattern (Tabb et al., 2004). The azole antagonist HipHop pharmacophore (Fig. 3B) suggests that two hydrogen bond acceptor features, a hydrophobic feature, and a ring aromatic (hydrophobic) feature are in common across the three molecules. This seems to indicate a balance between hydrophobic and hydrogen bonding features, which is in agreement with the proportions of steric and electrostatic fields from the biphenyl CoMFA model. As the PXR agonist and antagonist pharmacophores developed in this study are subtly different in their requirement for hydrophobic and hydrogen bonding features, this provides further evidence for likely different binding sites in PXR.

Azoles such as ketoconazole are widely known to interact with many cytochrome P450s in that the imidazole ring interacts with the heme. It is also appreciated that there is a difference in the interaction of fluconazole and ketoconazole with CYP51. This may be due to the additional hydrophobic interactions between ketoconazole and CYP51 having a K_d of 8 μM, whereas the smaller fluconazole is less active with a K_d of 120 μM (Matsuura et al., 2005). In contrast, both of these compounds are suggested as equipotent antagonists of PXR (Huang et al., 2007; Wang et al., 2007), which may indicate that the whole of the ketoconazole structure is unnecessary for antagonist activity. The HipHop pharmacophore for the 3 azole PXR antagonists confirms this in two ways. First, no pharmacophore features are mapped beyond and including the piperazine ring of ketoconazole. Second, the azole antagonist pharmacophore is substantially different from a recently published Hypogen pharmacophore for 26 azole and nonazole human CYP51 inhibitors that possessed three hydrophobic features and one hydrogen bond acceptor (Ekins et al., 2007), also suggesting that it may be possible to separate the PXR antagonism from P450 inhibition activities.

Docking Provides Insight into PXR Antagonist Binding. To further rationalize the possible fit of the azole antagonists in PXR, we have used an automated docking method called GOLD (Jones et al., 1997) that maintains the protein as rigid and flexibly docks the azole antagonists onto the outer surface of PXR. Definitive experimental mutagenesis data has shown ketoconazole docks in the AF-2 binding pocket and not in the ligand-binding pocket (Wang et al., 2007). Although it has been suggested that the azole ring could fit in the vicinity of the SRC-1 histidine, which interacts with Lys277 (Wang et al., 2007), no alignment of ketoconazole has previously been shown. The results in this present study suggest two different binding sites within close proximity to the region where SRC-1 binds the AF-2 site and, in particular, Lys277, on the outer surface of PXR. The scoring algorithm used with this method indicates that ketoconazole should have a slightly higher affinity than the other two azoles. We have selected one of the sites (Fig. 4A, site 2) as being more realistic based on the docking of the three azoles in this site. This binding site overlaps with the well known coactivator binding site (AF-2 region) in PXR, which shares similar hydrophobic features common across the nuclear receptor family. The AF-2 region in the nuclear receptor LBD has been shown to form a hydrophobic groove to accommodate the LXXLL motifs (L = leucine, X = any amino acid residue) or nuclear receptor boxes of p160 coactivators, as demonstrated by the recently solved cocrystal structures of nuclear receptor LBDs and LXXLL motif fragment complexes (Bledsoe et al., 2002; Wärnmark et al., 2002). The leucines of SRC-1 interacting with PXR are 690, 693, and 694. The docking study indicated that ketoconazole occupied two of the three subsites of this motif corresponding to Leu690 and Leu694. We also observed that azoles did not fill the site of Leu693. Thus, to achieve optimal antagonistic activity, the molecule should be able to cover all three leucine subsites, indicating that the azole affinity can be improved by rational structural design. The interactions between the PXR AF-2 region and its coactivators are essential to its transcriptional activation in the cells. We speculate that the three mentioned azole compounds occupy the AF-2 region and compete for binding with the PXR coactivator in a similar way, therefore disrupting this key protein-protein interaction essential for PXR activation. A structural homology model and molecular dynamics simulations have been used to assess the interaction of the corepressor SMRT, which was assumed to overlap with the coactivator site of PXR (Wang et al., 2006). Interactions identified with Lys259, Pro423, Glu427, and Glu270 were also identified in the current study for the antagonist ketoconazole.

The docking of ketoconazole further indicates that the whole of the molecule may not be important for interaction with PXR because the piperazine ring is solvent-exposed and protruded out of the binding groove (Fig. 4B) in agreement with the antagonist pharmacophore described above. Because the proposed antagonist binding sites are within range of Lys277, they would be affected if this residue changed, as

has been demonstrated with the double mutant at the 277 and 248 positions (Wang et al., 2007). Whether the double mutant also prevents antagonism by the other two smaller azoles is not known. We are now in a position to use the various computational models to suggest amino acid modifications and further test our different models.

The implications of the combination of approaches taken in this study are that to discover new potent PXR antagonists, we should focus on molecules that possess a balanced hydrophobic and hydrogen bonding profile and conform more closely to the antagonist pharmacophore and the identified binding site 2 in terms of size. Previous studies have suggested that some microtubule-stabilizing drugs displace the SMRT corepressor interaction with human PXR to enhance activation (Mani et al., 2005). This would also suggest another pharmacophore to be aware of in developing antagonists to avoid inadvertently targeting this site. Although the azoles miconazole and oxiconazole have been shown not to act as PXR antagonists (Wang et al., 2007), assessment of further azoles may be a starting point for extending this structure-activity relationship. For example itraconazole, terconazole, and voriconazole have greater than 90% similarity to fluconazole according to ChemFinder (CambridgeSoft, Cambridge, MA). Assessment of antagonist activity of modified azoles is also currently being investigated.

In summary, this study has combined experimental data and computational approaches to suggest plausible differences between the binding sites for human PXR agonists and antagonists using azoles, imidazoles, and steroidal and other diverse molecules. We have demonstrated that a series of novel imidazoles behave as human PXR agonists (as predicted a priori) and lower affinity antagonists, the latter probably the result of competitive inhibition of rifampicin binding in the LBD rather than at the AF-2 site. For the first time, we suggest that azole PXR antagonists may require more hydrogen bonding interactions than agonists (or at least a different distribution of these molecular features). We also suggest computationally that the azole antagonists would partially mimic, displace, or interfere with the coactivator SRC-1 binding at AF-2 or around this region on the outer surface of PXR, explaining the in vitro and mutagenesis data. Because both coactivators and corepressors possibly bind the same AF-2 or other sites, this would suggest that development of antagonists provides a therapeutic option for control of PXR transcription of target genes. The identification of sulforaphane as the first naturally occurring PXR antagonist (Zhou et al., 2007), and more recently the phytoestrogen coumestrol (Wang H, Li H, Moore LB, Maglich JM, Goodwin B, Ittopp OR, Wisely B, Creech K, Parks DJ, Collins JL, et al., submitted) may also indicate that a diverse array of molecules other than azoles could bind the coactivator or other sites at low micromolar affinity. In the latter case, coumestrol possesses two hydroxyl groups as well as several other oxygen atoms that could serve as hydrogen bond acceptors; this molecule fits three features of the antagonist pharmacophore (both hydrogen bond acceptors and the ring aromatic feature) but omits a hydrophobic feature (data not shown), suggesting that it may bind the same site as the azoles. It is noteworthy that sulforaphane fits to the hydrogen bond acceptor features only (data not shown), providing weaker evidence that it could bind the external PXR surface. Computational methods are widely available that could explore these proposed antagonist binding sites with a more extensive and diverse array of molecules in a higher throughput fashion than possible in vitro, to enable the discovery of "drug-like" molecules. This will be achieved by searching databases of known drugs or commercially available libraries of molecules with the pharmacophores, or docking the molecules into the sites identified in this study, followed by in vitro verification. Such an approach has been successfully applied to define new transporter inhibitors and substrates (Ekins et al., 2005; Chang et al., 2006) and is currently ongoing for PXR.

Acknowledgments

Dr. James Slama (University of Toledo, Toledo, OH) is gratefully acknowledged for synthesizing and providing the CDD imidazole compounds. We acknowledge John Ohrn and Dr. Shikha Varma (Accelrys, San Diego, CA) for efforts in making Catalyst available to us. S.E. acknowledges Dr. Maggie A. Z. Hupcey for moral support.

References

Bachmann K, Patel H, Batayneh Z, Slama J, White D, Posey J, Ekins S, Gold D, and Sambucetti L (2004) PXR and the regulation of apoA1 and HDL-cholesterol in rodents. *Pharmacol Res* **50:**237–246.

Bertilsson G, Heidrich J, Svensson K, Asman M, Jendeberg L, Sydow-Backman M, Ohlsson R, Postlind H, Blomquist P, and Berkenstam A (1998) Identification of a human nuclear receptor defines a new signaling pathway for CYP3A induction. *Proc Natl Acad Sci U S A* **95:**12208–12213.

Bledsoe RK, Montana VG, Stanley TB, Delves CJ, Apolito CJ, McKee DD, Consler TG, Parks DJ, Stewart EL, Willson TM, et al. (2002) Crystal structure of the glucocorticoid receptor ligand binding domain reveals a novel mode of receptor dimerization and coactivator recognition. *Cell* **110:**93–105.

Blumberg B, Sabbagh W, Jr., Juguilon H, Bolado J Jr, van Meter CM, Ong ES, and Evans RM (1998) SXR, a novel steroid and xenobiotic-sensing nuclear receptor. *Genes Dev* **12:**3195–3205.

Chang C, Ekins S, Bahadduri P, and Swaan PW (2006) Pharmacophore-based discovery of ligands for drug transporters. *Adv Drug Del Rev* **58:**1431–1450.

Clement OO and Mehl AT (2000) HipHop: pharmacophore based on multiple common-feature alignments, in *Pharmacophore Perception, Development, and Use in Drug Design* (Guner OF ed) pp 69–84, IUL, San Diego.

Coumol X, Diry M, and Barouki R (2002) PXR-dependent induction of human CYP3A4 gene expression by organochlorine pesticides. *Biochem Pharmacol* **64:** 1513–1519.

Cramer RD, Patterson DE, and Bunce JD (1988) Comparative molecular field analysis (COMFA). 1. Effect of shape on binding of steroids to carrier proteins. *J Am Chem Soc* **110:**5959–5967.

Ding X and Staudinger JL (2005) Induction of drug metabolism by forskolin: the role of the pregnane X receptor and the protein kinase a signal transduction pathway. *J Pharmacol Exp Ther* **312:**849–856.

Drocourt L, Pascussi JM, Assenat E, Fabre JM, Maurel P, and Vilarem MJ (2001) Calcium channel modulators of the dihydropyridine family are human pregnane X receptor activators and inducers of CYP3A, CYP2B, and CYP2C in human hepatocytes. *Drug Metab Dispos* **29:**1325–1331.

Dussault I, Lin M, Hollister K, Wang EH, Synold TW, and Forman BM (2001) Peptide mimetic HIV protease inhibitors are ligands for the orphan receptor SXR. *J Biol Chem* **276:**33309–33312.

Ekins S, Andreyev S, Ryabov A, Kirillov E, Rakhmatulin EA, Sorokina S, Bugrim A, and Nikolskaya T (2006) A combined approach to drug metabolism and toxicity assessment. *Drug Metab Dispos* **34:**495–503.

Ekins S and Erickson JA (2002) A pharmacophore for human pregnane-X-receptor ligands. *Drug Metab Dispos* **30:**96–99.

Ekins S, Johnston JS, Bahadduri P, D'Souzza VM, Ray A, Chang C, and Swaan PW (2005) In vitro and pharmacophore based discovery of novel HPEPT1 inhibitors. *Pharm Res* **22:**512–517.

Ekins S, Mankowski DC, Hoover DJ, Lawton MP, Treadway JL, and Harwood HJ Jr. (2007) Three-dimensional quantitative structure-activity relationship analysis of human CYP51 inhibitors. *Drug Metab Dispos* **35:**493–500.

Ekins S, Mirny L, and Schuetz EG (2002) A ligand-based approach to understanding selectivity of nuclear hormone receptors PXR, CAR, FXR, LXRα and LXRβ. *Pharm Res* **19:**1788–1800.

El-Sankary W, Gibson GG, Ayrton A, and Plant N (2001) Use of a reporter gene assay to predict and rank the potency and efficiency of CYP3A4 inducers. *Drug Metab Dispos* **29:**1499–1504.

Goodwin B, Moore LB, Stoltz CM, McKee DD, and Kliewer SA (2001) Regulation of the human CYP2B6 gene by the nuclear pregnane X receptor. *Mol Pharmacol* **60:**427–431.

Hamid R, Rotshteyn Y, Rabadi L, Parikh R, and Bullock P (2004) Comparison of alamar blue and MTT assays for high through-put screening. *Toxicol In Vitro* **18:**703–710.

Huang H, Wang H, Sinz M, Zoeckler M, Staudinger J, Redinbo MR, Teotico DG, Locker J, Kalpana GV, and Mani S (2007) Inhibition of drug metabolism by blocking the activation of nuclear receptors by ketoconazole. *Oncogene* **26:**258–268.

Jacobs MN (2004) In silico tools to aid risk assessment of endocrine disrupting chemicals. *Toxicology* **205:**43–53.
Jones G, Willett P, Glen RC, Leach AR, and Taylor R (1997) Development and validation of a genetic algorithm for flexible docking. *J Mol Biol* **267:**727–748.
Kliewer SA, Moore JT, Wade L, Staudinger JL, Watson MA, Jones SA, McKee DD, Oliver BB, Willson TM, Zetterstrom RH, et al. (1998) An orphan nuclear receptor activated by pregnanes defines a novel steroid signalling pathway. *Cell* **92:**73–82.
Krasowski MD, Yasuda K, Hagey LR, and Schuetz EG (2005a) Evolution of the pregnane X receptor: adaptation to cross-species differences in biliary bile salts. *Mol Endocrinol* **19:**1720–1739.
Krasowski MD, Yasuda K, Hagey LR, and Schuetz EG (2005b) Evolutionary selection across the nuclear hormone receptor superfamily with a focus on the NR1I subfamily (vitamin D, pregnane X, and constitutive androstane receptors). *Nucl Recept* **3:**2.
Leesnitzer LM, Parks DJ, Bledsoe RK, Cobb JE, Collins JL, Consler TG, Davis RG, Hull-Ryde EA, Lenhard JM, Patel L, et al. (2002) Functional consequences of cysteine modification in the ligand binding sites of peroxisome proliferator activated receptors by GW9662. *Biochemistry* **41:**6640–6650.
Lehmann JM, McKee DD, Watson MA, Wilson TM, Moore JT, and Kliewer SA (1998) The human orphan receptor PXR is activated by compounds that regulate CYP3A4 gene expression and cause drug interactions. *J Clin Invest* **102:**1016–1023.
Lemaire G, de Sousa G, and Rahmani R (2004) A PXR reporter gene assay in a stable cell culture system: CYP3A4 and CYP2B6 induction by pesticides. *Biochem Pharmacol* **68:**2347–2358.
Luo G, Cunningham M, Kim S, Burn T, Lin J, Sinz M, Hamilton GA, Rizzo C, Jolley S, Gilbert D, et al. (2002) CYP3A4 induction by drugs: correlation between a pregnane X receptor reporter gene assay and CYP3A4 expression in human hepatocytes. *Drug Metab Dispos* **30:**795–804.
Mani S, Huang H, Sundarababu S, Liu W, Kalpana G, Smith AB, and Horwitz SB. Activation of the steroid and xenobiotic receptor (human pregnane X receptor) by nontaxane microtubule-stabilizing agents. *Clin Cancer Res* **11:**6359–6369.
Masuyama H, Hiramatsu Y, Kunitomi M, Kudo T, and MacDonald PN (2000) Endocrine disrupting chemicals, phthalic acid and nonylphenol, activate pregnane X receptor-mediated transcription. *Mol Endocrinol* **14:**421–428.
Masuyama H, Inoshita H, Hiramatsu Y, and Kudo T (2002) Ligands have various potential effects on the degradation of pregnane X receptor by proteasome. *Endocrinology* **143:**55–61.
Matsuura K, Yoshioka S, Tosha T, Hori H, Ishimori K, Kitagawa T, Morishima I, Kagawa N, and Waterman MR (2005) Structural diversities of active site in clinical azole-bound forms between sterol 14α-demethylases (CYP51s) from human and Mycobacterium tuberculosis. *J Biol Chem* **280:**9088–9096.
Moore JT and Kliewer SA (2000) Use of the nuclear receptor PXR to predict drug interactions. *Toxicology* **153:**1–10.
Moore LB, Goodwin B, Jones SA, Wisely GB, Serabjit-Singh CJ, Willson TM, Collins JL, and Kliewer SA (2000) St John's wort induces hepatic drug metabolism through activation of the pregnane X receptor. *Proc Natl Acad Sci U S A* **97:**7500–7502.
Mu Y, Stephenson CR, Kendall C, Saini SP, Toma D, Ren S, Cai H, Strom SC, Day BW, Wipf P, et al. (2005) A pregnane X receptor agonist with unique species-dependent stereoselectivity and its implications in drug development. *Mol Pharmacol* **68(2):**403–413.
Mu Y, Zhang J, Zhang S, Zhou HH, Toma D, Ren S, Huang L, Yaramus M, Baum A, Venkataramanan R, et al. (2006) Traditional Chinese medicines wu wei zi (*Schisandra chinensis* baill) and gan cao (*Glycyrrhiza uralensis* fisch) activate pregnane X receptor and increase warfarin clearance in rats. *J Pharmacol Exp Ther* **316:**1369–1377.
Rühl R (2005) Induction of PXR-mediated metabolism by beta-carotene. *Biochim Biophys Acta* **1740:**162–169.
Rühl R, Sczech R, Landes N, Pfluger P, Kluth D, and Schweigert FJ (2004) Carotenoids and their metabolites are naturally occurring activators of gene expression via the pregnane X receptor. *Eur J Nutr* **43:**336–343.
Schuetz E and Strom S (2001) Promiscuous regulator of xenobiotic removal. *Nat Med* **7:**536–537.
Schuster D, Laggner C, Steindl TM, Palusczak A, Hartmann RW, and Langer T (2006) Pharmacophore modeling and in silico screening for new P450 19 (aromatase) inhibitors. *J Chem Inf Model* **46:**1301–1311.
Sinz M, Kim S, Zhu Z, Chen T, Anthony M, Dickinson K, and Rodrigues AD (2006) Evaluation of 170 xenobiotics as transactivators of human pregnane X receptor (hPXR) and correlation to known CYP3A4 drug interactions. *Curr Drug Metab* **7:**375–388.
Sonoda J, Chong LW, Downes M, Barish GD, Coulter S, Liddle C, Lee CH, and Evans RM (2005) Pregnane X receptor prevents hepatorenal toxicity from cholesterol metabolites. *Proc Natl Acad Sci U S A* **102:**2198–2203.
Staudinger J, Liu Y, Madan A, Habeebu S, and Klaassen CD (2001a) Coordinate regulation of xenobiotic and bile acid homeostasis by pregnane X receptor. *Drug Metab Dispos* **29:**1467–1472.
Staudinger JL, Goodwin B, Jones SA, Hawkins-Brown D, MacKenzie KI, LaTour A, Liu Y, Klaassen CD, Brown KK, Reinhard J, et al. (2001b) The nuclear receptor PXR is a lithocholic acid sensor that protects against liver toxicity. *Proc Natl Acad Sci U S A* **98:**3369–3374.
Synold TW, Dussault I, and Forman BM (2001) The orphan nuclear receptor SXR coordinately regulates drug metabolism and efflux. *Nat Med* **7:**584–590.
Tabb MM, Kholodovych V, Grun F, Zhou C, Welsh WJ, and Blumberg B (2004) Highly chlorinated PCBs inhibit the human xenobiotic response mediated by the steroid and xenobiotic receptor (SXR). *Environ Health Perspect* **112:**163–169.
Takeshita A, Inagaki K, Igarashi-Migitaka J, Ozawa Y, and Koibuchi N (2006) The endocrine disrupting chemical, diethylhexyl phthalate, activates MDR1 gene expression in human colon cancer LS174T cells. *J Endocrinol* **190:**897–902.
Takeshita A, Koibuchi N, Oka J, Taguchi M, Shishiba Y, and Ozawa Y (2001) Bisphenol-A, an environmental estrogen, activates the human orphan nuclear receptor, steroid and xenobiotic receptor-mediated transcription. *Eur J Endocrinol* **145:**513–517.
Takeshita A, Taguchi M, Koibuchi N, and Ozawa Y (2002) Putative role of the orphan nuclear receptor SXR (steroid and xenobiotic receptor) in the mechanism of CYP3A4 inhibition by xenobiotics. *J Biol Chem* **277:**32453–32458.
Ung CY, Li H, Yap CW, and Chen YZ (2007) In silico prediction of pregnane X receptor activators by machine learning approaches. *Mol Pharmacol* **71:**158–168.
Wang CY, Li CW, Chen JD, and Welsh WJ (2006) Structural model reveals key interactions in the assembly of the pregnane X receptor/corepressor complex. *Mol Pharmacol* **69:**1513–1517.
Wang H, Huang H, Li H, Teotico DG, Sinz M, Baker SD, Staudinger J, Kalpana G, Redinbo MR, and Mani S (2007a) Activated PXR is a target for ketoconazole and its analogs. *Clin Cancer Res* **13:**2488–2495.
Wärnmark A, Treuter E, Gustafsson JA, Hubbard RE, Brzozowski AM, and Pike AC (2002) Interaction of transcriptional intermediary factor 2 nuclear receptor box peptides with the coactivator binding site of estrogen receptor α. *J Biol Chem* **277:**21862–21868.
Watkins RE, Davis-Searles PR, Lambert MH, and Redinbo MR (2003a) Coactivator binding promotes the specific interaction between ligand and the pregnane X receptor. *J Mol Biol* **331:**815–828.
Watkins RE, Maglich JM, Moore LB, Wisely GB, Noble SM, Davis-Searles PR, Lambert MH, Kliewer SA, and Redinbo MR (2003b) 2.1A crystal structure of human PXR in complex with the St John's Wort compound hyperforin. *Biochemistry* **42:**1430–1438.
Watkins RE, Noble SM, and Redinbo MR (2002) Structural insights into the promiscuity and function of the human pregnane X receptor. *Curr Opin Drug Discov Dev* **5:**150–158.
Watkins RE, Wisely GB, Moore LB, Collins JL, Lambert MH, Williams SP, Willson TM, Kliewer SA, and Redinbo MR (2001) The human nuclear xenobiotic receptor PXR: structural determinants of directed promiscuity. *Science* **292:**2329–2333.
Waxman DJ (1999) P450 gene induction by structurally diverse xenochemicals: central role of nuclear receptors CAR, PXR, and PPAR. *Arch Biochem Biophys* **369:**11–23.
Xue Y, Chao E, Zuercher WJ, Willson TM, Collins JL, and Redinbo MR (2007a) Crystal structure of the PXR-T1317 complex provides a scaffold to examine the potential for receptor antagonism. *Bioorg Med Chem* **15:**2156–2166.
Xue Y, Moore LB, Orans J, Peng L, Bencharit S, Kliewer SA, and Redinbo MR (2007b) Crystal structure of the pregnane X receptor-estradiol complex provides insights into endobiotic recognition. *Mol Endocrinol* **21:**1028–1038.
Zhou C, Poulton EJ, Grun F, Bammler TK, Blumberg B, Thummel KE, and Eaton DL (2007) The dietary isothiocyanate sulforaphane is an antagonist of the human steroid and xenobiotic nuclear receptor. *Mol Pharmacol* **71:**220–229.
Zhou C, Tabb MM, Sadatrafiei A, Grun F, and Blumberg B (2004) Tocotrienols activate the steroid and xenobiotic receptor, SXR, and selectively regulate expression of its target genes. *Drug Metab Dispos* **32:**1075–1082.
Zhu Z, Kim S, Chen T, Lin JH, Bell A, Bryson J, Dubaquie Y, Yan N, Yanchunas J, Xie D, et al. (2004) Correlation of high-throughput pregnane X receptor (PXR) transactivation and binding assays. *J Biomol Screen* **9:**533–540.

Address correspondence to: Dr. Sean Ekins, ACT LLC, 601 Runnymede Avenue, Jenkintown, PA 19046. E-mail: ekinssean@yahoo.com